Ultrafast Phase Grating Studies of Heme Proteins: Observation of the Low-Frequency Modes Directing Functionally Important Protein Motions

John Deàk,[†] Hui-Ling Chiu,[†] Caroline M. Lewis, and R. J. Dwayne Miller*

Departments of Chemistry and Physics, 80 St. George Street, University of Toronto, Toronto, Ontario, M5S-1A1 Canada

Received: December 11, 1997; In Final Form: April 13, 1998

Transient phase grating spectroscopy has been used to study the tertiary global protein motions involved with the ligated to deligated conformational transition of carboxymyoglobin (MbCO) from 100 fs to 2 ns. Using counterpropagating beam geometries and monitoring the phase of the acoustics generated by the protein motion, it was possible to obtain picosecond resolution to observe the low-frequency acoustic-like modes of the protein coupled to the bond dissociation process. The asymmetric three-dimensional structure of the protein is expected to direct the reaction forces to specific displacements important to function. This anisotropic force/displacement was directly observed through the polarization analysis of the protein motion and induced material birefringence. These studies were complemented by a study of the absorption anisotropy to provide a probe of relaxation processes local to the heme binding site and epicenter of the reaction forces. The protein photoacoustics demonstrated that the dominant displacement or strain along the reaction coordinate develops on a 2 ps time scale. From the polarization analysis, the most significant strain component is parallel to the heme plane, which is consistent with translation of the F α-helix parallel to the heme plane as part of the allosteric core of the protein motions. The dynamics for the global protein motion and relaxation of the protein in the vicinity of the heme show essentially a 1:1 correspondence in dynamics. From the observed dynamics for the protein strain, amplitude, and two-point spatial correlation of the motion, it is concluded that the dominant coupling coefficient of the reaction forces is to the low-frequency collective modes of the protein. This mechanism is discussed within the context of an efficient mechanism for propagating functionally important protein motions and directing the system along the correct seam in this highly complex potential energy surface.

I. Introduction

The heme proteins, myoglobin and hemoglobin, serve an important function as the oxygen transport agents in the muscle and blood, respectively. Myoglobin is monomeric, whereas hemoglobin is a tetramer comprised of two different pairs of heme protein subunits similar in structure to myoglobin. The quaternary structure of hemoglobin imparts a cooperative effect between the subunits which enhances oxygen transport and has become the classic example for molecular cooperativity in biological systems.[1] Detailed single-crystal structure determinations have found that there are significant changes in structure accompanying changes in oxygenation that occur at both the tertiary and quaternary level.[2] The spatial separation between the four heme binding sites in hemoglobin is approximately 30 Å. In the absence of the surrounding protein, the oxygen binding at the hemes would be uncorrelated at this effective density for a purely solution process. The protein's structural changes form a strongly coupled system in which the tertiary relaxation is cascaded into the quaternary structural transition.[1−5] These structural changes provide a mechanism by which the reaction forces at one site can be coupled to an adjacent site to modify the reaction rate through structurally induced changes in the activation barrier. If one heme subunit loses an oxygen, the adjacent heme is more likely to lose its oxygen, and vice versa. In this manner, the structural changes form a synergistic feedback loop in which the system responds dynamically, nonlinearly, to changes in oxygen pressure. The net effect is that the pickup and transport of oxygen are significantly enhanced over monomeric oxygen-carrying heme proteins. The whole process forms a model system for understanding the general phenomena of allosteric regulation and molecular cooperativity in biological systems.

The structural relaxation convolved to the $Fe-O_2$ reaction coordinate involves the displacement to varying degrees of virtually all the atoms of the protein, i.e., the motion of thousands of atoms.[2] The mechanics of the coupling of the reaction forces between heme sites represents an intriguing question with respect to understanding this process from a microscopic level. The reaction forces involved in the bond formation between the iron and oxygen develop on an atomic level and must become spatially distributed globally to displace atoms on the mesoscopic scale appropriate to its biological function. The driving force for these highly correlated motions is derived from just a single bond, yet is capable of displacing some 10^3 to 10^4 degrees of freedom. From a simple consideration of the number of degrees of freedom coupled to the reaction coordinate and the observed dynamics for this and related biological processes, it is clear that these functionally important protein motions do not occur through random thermal sampling of the entire reaction phase space. The reaction forces must be highly directed into the specific motions that are integral to molecular cooperativity. What makes this question even more intriguing is that proteins are highly associated systems in which

[†] Department of Chemistry, University of Rochester, Rochester, NY 14627.

S1089-5647(98)00492-1 CCC: $15.00
Published on Web 08/05/1998

the potential energy surface contains a myriad of local minima.[6] How does the system avoid becoming trapped in local minima along the structural relaxation coordinate?

For systems as complex as proteins, it is useful to begin with a consideration of the basic elements of the problem. The binding of oxygen to the heme iron is an example of a condensed-phase reaction in which the globin surrounding the heme binding site can be viewed as the bath.[7] As with all condensed-phase reactions, the nuclear motion along the reaction coordinate involves coupling, of various degrees, to all the bath modes. In this case, the bath modes are related to the thermal fluctuations of the protein which enable the protein to sample different nuclear configurations. These motions consist of high-frequency motions (>60 cm^{-1}) which are more localized, to low-frequency collective modes ($1-60$ cm^{-1}) involving the entire protein at the lowest frequencies (e.g., acoustic breathing motions), to relaxation modes (<1 cm^{-1}) and thermally activated relaxation between different conformations.[7-9] The latter relaxation can involve time scales from nanoseconds to milliseconds depending on the barriers separating different conformations. With respect to ligand binding at the heme site, the motions with the greatest influence on the reaction are those that assist the displacement of the iron from the out-of-plane position in the heme porphyrin ring (deoxy configuration) to the in-plane (oxy) configuration. This is the motion that leads the system through the reaction saddle point between bond formation and dissociation. In transition-state theory, the nuclear prefactor that determines the rate of passage through this region is dominated by the highest frequency mode which leads to the greatest degree of relaxation along the nuclear potential energy surface.[10] This motion along the bond formation coordinate, from high frequency through to conformational relaxation, must ultimately produce atomic displacements that are part of the allosteric mechanism. This mechanism, in turn, must involve atomic displacements at the protein interface in order for the reaction at one site to affect the binding efficacy of a neighboring protein. Otherwise, the two reaction coordinates are shielded from one another. Displacements in the interfacial region transfer forces from one site to another and enable the activation barrier of an adjacent site to be modulated by the state of ligation of a neighboring protein.

The question, then, is the following: what is the mechanism by which the reaction forces of bond formation at the iron site lead to the atomic displacements that establish the molecular communication pathway? Due to the three-dimensional nature of the interatomic interactions, displacements at the interface cannot occur without affecting other atomic positions to a certain degree throughout the entire protein; i.e., there is an associated change in reaction volume. In mechanics, a change in volume is defined as strain ($\Delta V/V$) and is the three-dimensional equivalent to the normalized displacement of a one-dimensional spring.[11] The response of the protein to the reaction forces (stress) will lead to anisotropic strain in the protein structure. The development of protein strain with bond formation/dissociation will have contributions from all components to the protein motion. Different motions will experience larger displacements which depend on the relative relaxation energy associated with the particular motion. The question can be rephrased to the following: what are the coupling coefficients of the different modes/relaxations to the protein strain coordinate? Is there a dominant mechanism to the protein motion that directs the functionally important motions; i.e., are there modes or relaxation processes with larger coupling coefficients to the reaction coordinate?

In this regard, there are two limiting cases with respect to the length scale and dynamics of the protein response function to the reaction at the heme site.[7,12,13] In one scenario, the reaction forces lead to localized displacements along the protein strain coordinate. For example, the length scale of any given relaxation component in this particular scenario could be on the order of one amino acid residue (e.g., relaxation at the proximal histidine position). Localized motions require diffusive relaxation processes, and the protein strain would only develop through the highly distributed kinetics of the protein response function. Given the highly associated nature of proteins, this part of the protein response function is often modeled in analogy to glass relaxation dynamics[14] and represents what will be referred to as the *long time limit* to the motions. At the other extreme, the dominant contribution to the protein displacements could involve the nondiffusive motions which occur within the *short time limit* to the protein dynamics. There is very little information on the short time dynamics of the protein response function to the reaction forces. On short time scales ($<10^{-11}$ s), the atomic fluctuations are more strongly correlated to the secondary and tertiary structure, and a modal description for the protein motions becomes more appropriate. This statement follows the same justification for a modal treatment to model the short time behavior of liquids.[15-19] There is, however, an important distinction. In the liquid state, the molecules are interacting through relatively weak forces such that the dynamics can be properly described with either a localized basis or a collective coordinate (modes). For proteins, the atoms are covalently bonded, and the overall correlation length scale is determined by much stronger forces than the intermolecular forces in liquids. The use of a modal description for the short time dynamics of protein motions is more rigorous than it is for liquids. In the short time limit, the reaction forces are expected to displace low-frequency collective modes inherent to the protein structure, and the protein strain would develop more globally. In contrast to the localized strain picture above, the protein response would be characterized by the nanometer length scales of the protein or correlated displacements extending over several (up to tens of) amino acid residues. In this case, the dynamics would not be highly distributed but more closely related to recent observations of inertial components to solvent relaxation.[20,21] If the short time dynamics dominate the protein relaxation, the largest strain would develop in the first few picoseconds, corresponding to the displacement of the protein's inherent low-frequency collective modes in response to the reaction forces.

These two extreme limits highlight that protein relaxation has both a frequency and an associated length scale; i.e., the mechanical response of the protein to the reaction forces has both an ω and $\mathbf{k}$ dependence.[7] By using time domain probes sensitive to different length scales of the protein relaxation, the degree of coupling of the reaction forces to the different frequency components available to the protein motion can be determined. This information determines the length scale of the acting forces and the mechanism by which the forces are transmitted from one reaction coordinate to another.

The relevant time scales to this problem span the 100 fs range, associated with the bond breaking event (10^{-13} s) at the reaction saddle point, to microseconds and longer to cover the conformational relaxation phase. To access information on the fastest protein relaxation processes and address the above issues, optical methods are needed to initiate the functional response. In this regard, the oxy to deoxy tertiary structure transition in hemoglobin and myoglobin can be initiated optically through the

photodissociation of the ligand from the heme group.[22] Time domain optical studies have shown that photoexcitation of the heme group leads to ligand dissociation within 50 fs, with essentially unit quantum yield.[23] Subsequent relaxation from this nonequilibrium condition serves as an excellent model for the protein relaxation dynamics involved in the thermally sampled reaction saddle point. As long as the interatomic potentials are all near harmonic limits, the dynamics will be identical to that involved in the actual biological process. For systems as large as heme proteins, the majority of displacements fall within this limit.[24]

A variety of time domain spectroscopies have shown that these different motions occur over a wide range of time scales, from 300 fs to microseconds (aqueous room-temperature conditions).[23,25−30] Oxygen shows highly nonexponential geminate recombination in this dynamic range,[31] whereas there is less than 5% recombination with CO.[32] For this reason, CO is typically used to explore the long time limit of the protein relaxation. In addition, most of the spectroscopies applied to this problem rely upon the heme group as an indirect probe of the protein motion as these motions perturb the heme's electronic state. These measurements have given detailed dynamical information on structural rearrangements near the heme group, but those motions that do not strongly perturb the heme's electronic transition, or related probes of the heme pocket, are not easily detected. Ideally, one would like to be able to probe the time evolution of the protein strain directly. In addition, it would be highly desirable to follow the low-frequency modes of the protein which are coupled to the bond formation/dissociation coordinate and determine the initial barrier crossing dynamics which set the whole process in motion.

Transient phase grating spectroscopy has been shown to be an extremely sensitive probe of protein relaxation.[7,12,13] The observable in the phase grating experiment is the photoinduced changes in index of refraction and has been treated extensively in a number of applications.[33−37] With respect to heme proteins, the development of protein strain along the reaction coordinate involves material displacement which alters the index of refraction. This change in index of refraction can be thought of as a density-dependent effect. Due to the interferometric nature of the experiment, changes in effective radius of the protein of less than 0.01 Å (strain of less than 10^{-4}) can be detected. The key distinction of this spectroscopy is that it provides a direct observation of the protein strain which is the dynamic variable of central interest in molecular cooperativity (vide supra).

Previous studies of carboxymyoglobin (MbCO) and carboxyhemoglobin (HbCO) have shown that the dominant contribution to the protein strain (>80%) develops in less than 10 ps, within the 10 ps to 10 ns dynamic window studied.[7] It was argued based on the close relationship of the strain dynamics to other probes of relaxation near the heme that the initial phase of the protein relaxation involved significant coupling of the reaction forces to the collective modes of the protein structure.[7,12,13] This earlier work did not have sufficient time resolution to unambiguously establish this connection. In the present work, the time resolution has been improved to 100 fs so that even the fastest relaxation processes can be studied. In addition, studies have been conducted to take advantage of the fact that proteins in general lack a center of symmetry. The highly anisotropic nature of the protein structure is in essence how reaction forces are directed along specific channels in the protein function. It is expected that the development of strain in heme proteins should be highly anisotropic and geared toward focusing forces from the heme binding site to the interface region. This expected anisotropy has been verified and directly probed in these studies by using a polarization analysis of the protein strain. To further verify that the index of refraction changes are related to global changes in protein strain, counterpropagating beam geometries have been employed to enable a direct probe of the protein strain driven acoustics in the 10 GHz range. The explicit use of the acoustic phase information has enabled true picosecond resolution to the translational components of the protein motion (protein photoacoustics). In addition, absorption anisotropy studies of the band III transition have been conducted to provide an independent probe of the relaxation at the heme site. These studies provide a general approach for determining the relative importance of low-frequency modes in functionally important protein motions. The present work focuses on MbCO to isolate the tertiary structural relaxation involved in the process. As will be discussed below, the observed dynamics, acoustic nature of the protein motions, and two point spatial correlation of the dynamics provide a direct evaluation of the importance of the collective mode mechanism in propagating structural changes coupled to the iron−ligand dissociation coordinate. It is these functionally important motions that ultimately form the structural feedback loop behind allosteric regulation in hemoglobin.

II. Experimental Section

The general features of the grating setup have been described in detail elsewhere.[13,33] In this work, three different laser systems were employed. The probe wavelength dependence of the protein acoustics at 532 nm and 1.064 μm was determined with a mode-locked and Q-switched Nd^{3+}:YAG laser (140 ps pulse widths). The experimental setup has been described elsewhere.[13] The counterpropagating grating excitation beam studies at 585 nm were conducted with a synchronously amplified dye laser system. The dye laser was hybridly mode-locked with an intracavity saturable absorber and synchronously pumped by a mode-locked and frequency-doubled Nd^{3+}:YLF laser which also served as a seed for a Nd^{3+}:YLF regenerative amplifier. The regeneratively amplified pulses were also doubled and used to pump a two-stage Rhodamine 6G dye amplifier system which provided 10 μJ pulse energies with pulse widths of <1 ps, at a wavelength centered at 585 nm and repetition of 2 kHz. The simplest configuration for a counterpropagating beam geometry is to use the same wavelength for both the excitation and probe to facilitate meeting Bragg phase matching conditions. A 50% beam splitter and a partial reflector were used to generate the grating excitation and probe beams, respectively, and all the beams were vertically polarized. Separate delays were positioned in each beam arm to adjust the timing between the three pulses. A rapid scanning galvonometer optical delay line, electronically synchronized to the regenerative amplifier, was used for the probe to provide a total scan range for the probe delay of 150 ps. The probe was brought in slightly out of plane in the vertical direction, above the excitation beams, with the backscattered signal isolated with an iris and detected with a silicon photodiode, after approximately a meter path length from the sample to reduce the background scattered excitation. The wavelength of 585 nm was chosen to excite within the Q-band absorption feature of heme proteins and deposit the least excess thermal energy above the Fe−ligand bond energy as possible. The excitation beams were focused to a diameter of 300 μm and attenuated to a combined energy of 1 μJ, which corresponds to exciting on average 10% of the heme proteins within the excitation volume

defined by the excitation beam diameters. The probe was attenuated relative to the excitation by a factor of 20 and was focused to a spot size of 200 μm. The sample was housed in a rotating cell that ensured that each laser shot sampled a fresh spot.

The counterpropagating setup was used to directly study the protein acoustics. To study the protein relaxation processes with higher time resolution and to examine the protein anisotropy, a regeneratively amplified titanium:sapphire laser system was used. This system provided 100 fs, 760 nm pulses with energies of several hundred microjoules at a 1 kHz repetition rate. The wavelength of 760 nm was chosen to coincide with the maximum of the band III transition of the photoinduced deoxy heme proteins to minimize phase contributions to the grating signal from population terms. The 760 nm beam was separated into two beams with a 30%:70% beam splitter. The more intense beam was frequency doubled to provide the excitation, on the blue edge of the Soret transition at 380 nm, and the other beam was used as the probe. The grating excitation pulses were focused to a 250 μm diameter spot size with a probe spot size of 200 μm. The pump energy was kept below 1 μJ so as not to exceed a 10% bleach. Typically, the probe energy was kept below 300 nJ, and the grating was probed at the Bragg angle. For polarization analysis of the signal, the polarization of each beam was kept to 1 part in 10^4 contrast ratio with individual Glan-type polarizers. The explicit grating configuration consisted of two vertically polarized excitation pulses at 380 nm crossed at an angle in the horizontal plane (polarization orthogonal to grating wave vector) with the 760 nm probe polarized at various angles with respect to the excitation. In contrast to the counterpropagating studies, these studies are not concerned with the acoustic modulation of the signal per se but the dynamics of the protein relaxation dependent changes in the index of refraction and induced birefringence. To minimize acoustic modulations of this signal at short times, small angles of less than 4.5° between the excitation beams were used to increase the acoustic period out to the 5 ns range. Analysis of the associated acoustic modulation of the signal used longer delay times and angles of 11° between the excitation beams to give several acoustic oscillations of the diffracted signal over the scan range. For the short time dynamics, a rapid scanning galvanometer optical delay line was used, while longer delay times were produced with a motorized positioning table. To avoid depolarization effects from stray birefrigence in rotating samples, a flow cell was used in these studies. The cell was designed to also minimize nonresonant nonlinear interactions of the polarized light fields with the sample solvent and windows by using as small a path length as possible. The cell had a flow path length of 380 μm and used 500 μm thick UV grade fused silica windows.

The carboxylated form of the heme proteins was used for these studies to avoid complications from geminate recombination on the time scale of interest. Lyophilized horse heart myoglobin was purchased from Sigma. Solutions of MbCO in 0.1 M Tris buffer (pH = 6.9) were made by reducing the myoglobin with a 2-fold excess of sodium dithionite, under a nitrogen atmosphere, and then subjecting the protein to carbon monoxide until complete conversion was indicated via UV−vis spectroscopy. The deoxymyoglobin samples were prepared in the same way as the MbCO samples, terminating the preparation with the reduction of the heme. Heme octapeptide was obtained from cytochrome *c* as described by Kraehenbulh et al.[38] Carbon monoxide heme octapeptide was prepared by reducing the heme with a 5 times excess of dithionite, under a nitrogen atmosphere, and flowing carbon monoxide until complete conversion was indicated by UV−vis spectroscopy. All sample concentrations and sample path lengths were adjusted to provide an optical density of approximately 1 at the excitation wavelength. The different laser systems used to study these samples can be identified by the probe wavelength. The 532 nm and 1.064 μm probe wavelengths were generated using the mode-locked Q-switched YAG system; the 585 nm studies employed the regeneratively amplified dye laser, and the studies at 760 nm were conducted with the Ti:sapphire system.

III. Results and Discussion

Previous phase grating studies have shown that the photodissociation of the Fe−CO bond in heme proteins leads to the generation of a *nonthermal* acoustic wave of the grating wavevector.[7,12,13] The acoustic wave is driven by the material displacement which occurs as the protein relaxes from the oxy to deoxy tertiary structure. The protein strain amplitude is correlated to the amplitude of this nonthermal acoustic component. By comparing different proteins and carboxyhemes without the surrounding globin structure, it was demonstrated that this signal is derived from the relaxation of the globin. On the basis of the observed dynamics and magnitudes of the initial protein strain, it was argued that the forces derived from the bond-breaking event were coupled predominantly to the low-frequency collective modes of the protein.[7] A key test for this concept would be to directly observe the displacement of the low-frequency collective modes of the protein during the bond dissociation process. Toward this goal, we have investigated two new transient grating approaches to observing the lowest frequency modes coupled to the reaction coordinate. One method exploits the use of counterpropagating beam geometries to give picosecond time resolution to the photoinduced protein acoustics and casts out the acoustic modes involved in the bond-breaking event. The other method involves the use of a polarization analysis of the grating to directly observe the anisotropy of the evolving protein strain. This latter method affords even higher time resolution to the global protein motion.

The rationale for the counterpropagating studies is that this beam geometry gives the highest possible acoustic frequency using grating excitation and therefore the highest time resolution to the protein acoustics. The acoustic frequency ν_{ac} is given by the relation[33]

$$\nu_{ac} = (2n\upsilon_s \sin \theta_{ex}/2)/\lambda_{ex} \quad (1)$$

where n is the index of refraction, υ_s is the speed of sound, λ_{ex} is the excitation wavelength, and θ_{ex} is the angle between the excitation beams inside the refractive medium. The highest frequency for a given excitation wavelength is at $\theta_{ex} = 180°$ (i.e., counterpropagating excitation). This beam geometry prohibits the use of a nonresonant probe. Due to geometrical constraints, the phase matching conditions for diffraction can only be met by a probe of the same central wavelength, or within a narrow wavelength range, such that diffraction from both resonant and nonresonant grating source terms needs to be considered. In this case, there is a contribution to the signal from the spatially modulated population of excited molecules and the photoacoustics. The diffracted signal from this mixed grating condition is given by[13,33,39]

$$\eta = (2\pi/\lambda)^2\{(\Delta k_{ex})^2 + (\Delta n_{ex} + \Delta n_{ac})^2\}[G(\theta_{ex},\omega)] \quad (2)$$

where η is the diffracted light intensity ($\eta \ll 1$) assuming negligible attenuation of the probe, $G(\theta_{ex},\omega)$ is a constant

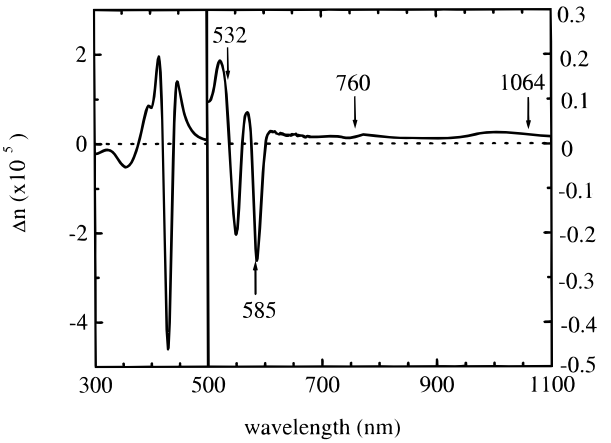

Figure 1. Kramers−Kronig analysis showing the probe wavelength dependence on the population grating contributions to the phase grating components. The left axis refers to the index of refraction change ($\times 10^5$) between 300 and 500 nm, and the right axis refers to the index of refraction change ($\times 10^5$) between 500 and 1100 nm. The different probe wavelengths studied to date are indicated by the arrrows.

correction factor from the plane wave approximation for finite Gaussian beams of radius ω and intersecting at an angle θ_{ex}, λ is the probe wavelength, Δk_{ex} is the peak−null spatial variation in the absorption (ΔOD) induced by the grating excitation at the probe wavelength, Δn_{ex} is the corresponding variation in the index of refraction, and Δn_{ac} is the periodic variation in the index of refraction due to density modulations associated with the photoacoustics. This latter term can be either positive or negative relative to the population phase grating contributions. The sign of the acoustic contribution only depends on whether the photoinduced density change corresponds to a dilation ($\Delta n_{ac} < 0$) or a contraction ($\Delta n_{ac} > 0$). In contrast, the sign of the population phase grating contribution (Δn_{ex}) depends on the probe wavelength. This contribution arises from the spatial modulation in absorption and the sign changes depending on whether the probe is on the blue ($\Delta n_{ex} < 0$) or red edge ($\Delta n_{ex} > 0$) of a dominant induced absorption feature.

The probe wavelength dependence of the population phase grating contribution can be determined by a Kramers−Kronig (K−K) analysis of the photoinduced change in the absorption spectrum. For myoglobin, the absorption difference spectrum becomes essentially indistinguishable from the equilibrium spectrum within 30 ps.[13,23] A K−K analysis of the population grating magnitude and sign, based on the equilibrium difference spectrum, is shown in Figure 1. In this figure the position of the different probe wavelengths studied to date are indicated by arrows. Representative data of the signal from MbCO at probe wavelengths of 1.064 μm, 760 nm, and 532 nm are shown in Figure 2. These figures show the MbCO data referenced to deoxyMb. In these studies, deoxyMb serves as the control for the pure thermal response. The excited state of deoxyMb undergoes rapid nonradiative relaxation to form a highly vibrationally excited ground state in less than a picosecond which reaches full equilibriation with the bath through rapid collisional exchange in less than 20 ps.[34,40] There is no photochemistry, and the photophysics involve solely photothermal effects. Thus, deoxyMb serves as a good control for separating the thermal response from photochemically induced structural relaxation.

It was not possible to have exactly the same grating fringe spacing for the different studies shown in Figure 2. To facilitate comparison of the protein driven acoustics for the different grating configurations, the data are plotted as a function of time

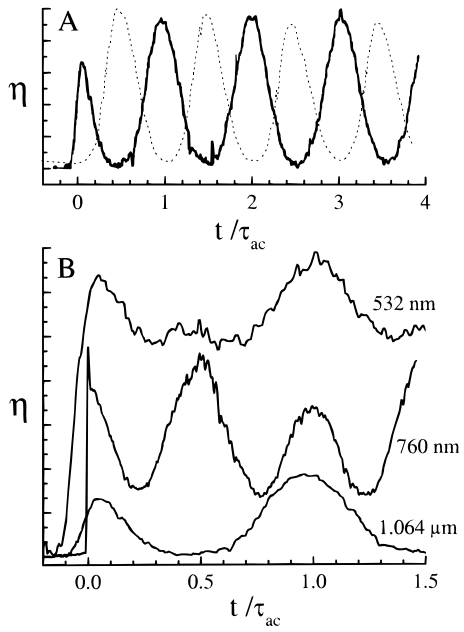

Figure 2. Experimental studies of the probe wavelength dependence. The data are plotted as a function of time normalized to the acoustic period (τ_{ac}) for MbCO (—) and deoxyMb (- - -). (A) Direct comparison of the protein-driven and thermally driven acoustics using 532 nm excitation and 1064 μm probe ($\tau_{ac} = 1$ ns, $\theta_{ex} = 20°$). The acoustic modulation of the diffracted signal for MbCO is 180° out of phase with the deoxyMb thermally driven acoustics (ref 12). For reference, the maxima in thermally driven acoustics occur at integral values of half an acoustic cycle. (B) Probe wavelength dependence. For $\lambda_{probe} =$ 760 nm, the excitation wavelength is 380 nm and $\tau_{ac} = 1.28$ ns ($\theta_{ex} =$ 11°). For $\lambda_{probe} = 532$ nm and 1.064 μm, the excitation wavelength is 532 nm with $\tau_{ac} = 1$ ns and $\theta_{ex} = 20°$ (ref 13).

normalized to the grating acoustic period (τ_{ac}). In comparing the data for MbCO and deoxyMb, there are a number of features to note. First, there is a different and distinctive acoustic signature for MbCO, relative to that of the purely thermal response of deoxyMb. This acoustic signature is associated with the protein relaxation following ligand dissociation. The difference is most readily observed at the 1.064 μm probe wavelength (Figure 2A) in which there is no discernible population grating terms, and only the acoustics are observed. (Δn_{ac} is the dominant term in eq 2.) There is a rapid rise in the diffracted signal due to the protein motion which is much faster than the thermal expansion response. The protein motion responsible for this signal drives a sound wave which modulates the signal 180° out of phase relative to the thermal wave. Studies of different heme proteins and control studies without the surrounding globin have shown that this acoustic wave is launched by the tertiary relaxation of the surrounding globin. Furthermore, studies at the zero thermal expansion point have demonstrated that this protein-driven sound wave is nonthermal.[7,12,13] This observation illustrates that the initial protein relaxation involves a volume change, i.e., it is acoustic in nature. From herein, this acoustic feature will be referred to as the protein wave.

The other probe wavelengths also show a significant contribution to the signal due to the protein driven acoustics (Figure 2B). Only the data for MbCO are shown in Figure 2B for clarity, as the deoxyMb acoustic waveform is the same as that shown in Figure 2A. For probe wavelengths at 532 and 760 nm, the acoustics appear on top of an offset which is due to the population grating contribution. This additional contribution arises from the changes in optical properties which follow photodissociation of MbCO to generate deoxyMb and leads to

a peak−null variation in the MbCO number density. This population grating term relaxes with CO recombination which occurs on the millisecond time scale. From Figures 1 and 2B (532 nm probe), the protein acoustic modulation adds to the signal at wavelengths at which the population phase grating components are positive which implies the protein driven sound wave involves an increase in the index of refraction. This point was confirmed by beating the protein wave against thermally generated acoustics.[12] The sign of the index change for the thermally driven acoustics is well-defined: thermal expansion leads to a decrease in density, and a corresponding decrease in the index of refraction, such that the peak−null difference in the index of refraction is negative. By increasing the thermal amplitude of the acoustics, through multiphoton processes, it was demonstrated that the protein wave and the thermal acoustics are opposite in sign. This finding is most simply interpreted as a net contraction following ligand dissociation which is consistent with previous findings from photoacoustic measurements with nanosecond resolution.[41] It should be noted that, for the 760 nm data, 380 nm excitation was used which deposits more excess energy as heat. The increased thermal component is responsible for the observed double beating and is similar to the previous studies in which the thermal component was increased by multiphoton absorption.

The most important discovery from the previous studies was that the protein strain appears to develop on a picosecond time scale and accounts for >80% of the protein relaxation.[12,13] Up-conversion of the diffracted signal at 1.064 μm has shown that the rise time is less than 10 ps.[42] The exact dynamics of the protein relaxation are important as this motion can be correlated potentially to specific modes and help elucidate the mechanism that couples the reaction forces to functionally important protein motions. Unfortunately, short-lived excited-state absorption (resonant contributions) and vibrational cooling of the excited heme complicated the signal at early time such that only an upper limit of 10 ps could be determined for the dominant relaxation components to the protein relaxation ($\tau_{relax} < 10$ ps). To avoid excited-state contributions to the signal and unambiguously correlate the dynamics to global protein relaxation, it would be desirable to observe solely the acoustics. This objective necessitates the use of counterpropagating beam geometries and specifically resolving the acoustic phase shift to achieve picosecond resolution.

These results are shown in Figure 3 for MbCO and deoxyMb using counterpropagating 585 nm pulses. There was considerable scattered light and associated noise in this experiment. To improve the signal-to-noise, a rapid scanner with a range of 150 ps was used to reduce the noise from slow laser drift (subhertz noise components). For this reason only the first acoustic modulation in the signal is shown (inset to Figure 3). The acoustic modulation for MbCO was found to be approximately the same near the zero thermal expansion point, whereas the deoxyMb acoustics significantly decreased in amplitude. This study shows the MbCO acoustic modulation is predominantly nonthermal and arises from the protein structural relaxation, as discussed above. The key thing to notice, however, is that the protein driven acoustics from MbCO now appear to be in phase with the pure thermal response of the deoxyMb data. Referring back to Figure 1, this result is expected at 585 nm as there is a sign change in the phase contribution from the population grating, and the magnitude is much larger relative to the other probe wavelengths. The population grating term (Δn_{ex}) at 585 nm is negative and opposite in sign to the protein acoustics. Due to the quadratic

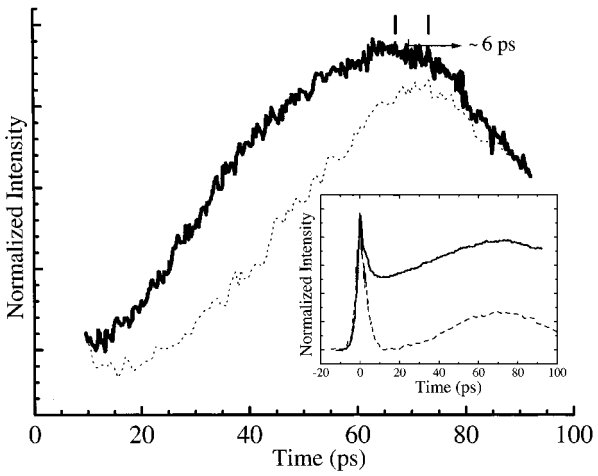

Figure 3. Counterpropagating grating studies with 585 nm excitation. The inset shows MbCO (—) data which is offset from the deoxyMb (- - -) control due to the population grating terms present for MbCO. The acoustics for MbCO now appear nearly in phase with the thermally driven acoustics due to the change in the population grating cross term. The acoustic component is amplified relative to the inset to illustrate the phase shift of 6 ps between the thermally driven acoustic wave of deoxyMb and the nonthermal protein driven acoustics which dominate the MbCO response.

nature of the grating signal, there is a cross term ($2\Delta n_{ex}\Delta n_{ac}$) which is readily seen by expanding the phase grating term (Δn^2) in eq 2. Relative to the other probe wavelengths, the cross term with the population grating causes the acoustic modulation to produce maxima in the diffracted signal which are now approximately temporally coincident with the thermally driven sound wave. The sign change in the population grating contribution compensates for the 180° phase shift between the thermally and protein-driven acoustic modulation of the diffracted signal at the other probe wavelengths and more readily enables a quantitative evaluation of the acoustic phase relationship of the two sound fields. That is, at the 585 nm probe wavelength, both the protein acoustics (through the change in sign of the population grating cross term) and the thermally driven acoustics produce maxima at approximately one-half an acoustic cycle. It is more convenient to compare the relative phase of two maxima rather than the relative phase of a minimum and a maximum when the signal modulation is 180° out of phase. In addition, the signal-to-noise is better at the maxima which increases the accuracy of this determination.

The most important feature of the data shown in Figure 3 is the phase of the acoustics. In direct comparison of the protein driven acoustics (MbCO) to the pure thermal response (deoxyMb), there is a 6 ps phase shift between the two acoustic waveforms. This difference is readily seen in the shift between the maxima in the acoustic modulation of the signal. The protein-driven sound field appears shifted to earlier time by this amount. This finding illustrates that the protein relaxation does in fact involve a volume change or the development of strain on a picosecond time scale. The dynamics of this motion can be determined by referencing the signal to the thermally driven acoustics in which the relaxation of excess energy to translation energy has been fully resolved by the work of Lian et al. to provide a known response function.[43] These workers found that the thermalization dynamics involved a Gaussian distribution with a 1/e value of 8 ps. This work agrees with our earlier studies of the vibrational to translational collisional exchange process[40] but was able to fully resolve the dynamics. If we use this observation as the source term for the thermal wave, the 6 ps shift between the thermally and protein-driven waves demon-

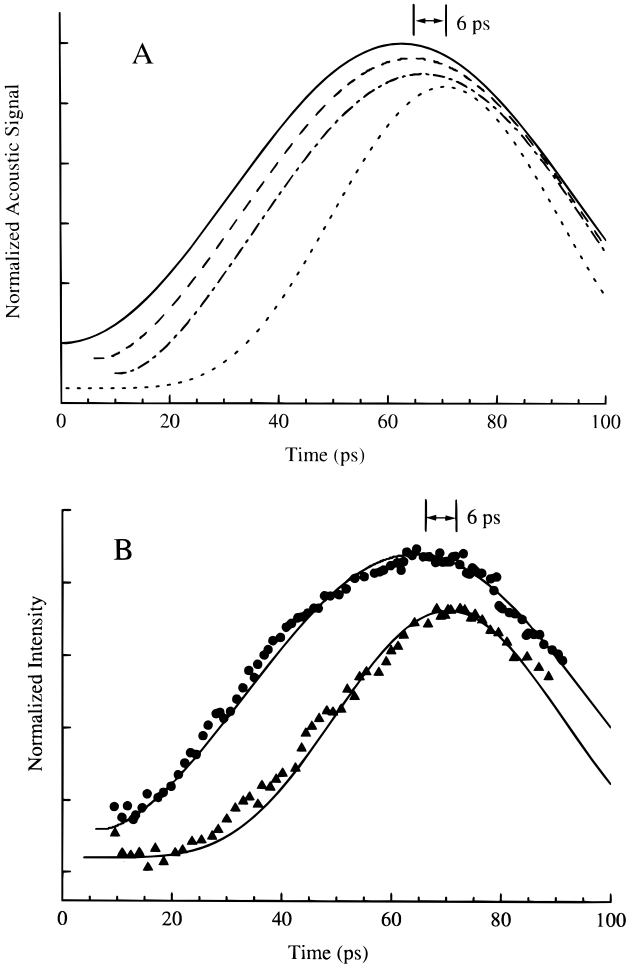

Figure 4. (A) Calculated acoustic response for thermal and structural relaxation driven sound fields. The thermal response was calculated based on the theory of Genberg et al. (ref 44) using an 8 ps thermalization time (dotted line). The corresponding calculations for the protein-driven sound waves, based on the theory of Puchenkov and Malkin (ref 45), for an instantaneous response (solid), a volume change of 2 ps (dashed), and 4 ps (dot−dash) for the protein relaxation are shown for comparison. (B) Direct comparison to the data shown in Figure 3. The structural relaxation time of 2 ps reproduces the observed 6 ps phase shift observed between the thermally driven sound fields of deoxyMb (triangles) and the protein driven waveform of MbCO (circles).

strates that the protein strain has a dominant component of approximately 2 ps.

To further illustrate this point, the dependence of the phase shift on the relaxation dynamics is shown in Figure 4. The thermally generated acoustic waveform for deoxyMb was calculated based on the exact analytical solutions to the coupled thermoelastic equations with a finite relaxation source term appropriate to the grating boundary conditions.[44] This response is calculated from the relation

$$\eta = \{C\{\omega^{-2}(1 - \cos \omega t) - (\gamma^2 + \omega^2)^{-1}[\gamma\omega^{-1} \sin \omega t - \cos \omega t + e^{-\gamma t}]\}\}^2 \quad (3)$$

where C is a constant depending on the heat capacity and the optoelastic constant and $\omega = 2\pi/\tau_{ac}$ and $1/\gamma$ is the relaxation time defining the nonradiative relaxation process of the excited state into translation energy of the bath. Thermal diffusion can be ignored in this problem. The protein-driven acoustic waveform was calculated based on the recent theory of Puchenkov and Malkin[45] for a volume driven acoustic wave. We extended their work to include the specific functional form of the time-dependent volume change. Following their formalism, the acoustics can be calculated from the dynamical equation for the density modulation $\delta = \rho - \rho_0$, caused here by a structural change in the protein:

$$\Delta\delta - \frac{1}{v_s^2}\frac{\partial^2\delta}{\partial t^2} = \frac{\rho_0}{v_s^2}\frac{\partial^2 V}{\partial t^2} \quad (4)$$

where V is the photoinduced relative volume change in the medium with the volume change in a single act of structural relaxation going as $\Delta v_0[1 - \exp(-t/\tau_{SR})]$. The dynamics of the protein strain are approximated by an effective structural relaxation time of τ_{SR}, and Δv_0 is the accompanying volume change of the protein. This response is convolved to the laser pulse and used to generate the forcing function for the acoustics (last term in eq 4).

The peak−null variation in the index of refraction due to the acoustics (Δn_{ac}) is proportional to the spatial modulation of the density calculated from the above equation. In the case of the MbCO grating experiment with a 585 nm probe, the acoustic signal beats against the population grating term (Δn_{ex}) which is more than 10 times larger at 585 nm than at the 1.064 μm probe wavelength. This cross term causes both the sign change and linearizes the acoustic signal. The relative magnitude of the population grating term (Δn_{ex}) was adjusted in the phase grating component (eq 2), and values larger than $2|\Delta n_{ac}|$ were found to reproduce the observed acoustic waveform within the signal-to-noise. Apart from this, the fit is insensitive to the magnitude of the excited-state term. Taking this effect of the population grating term into account, the best fits to the protein-driven acoustics, as derived from direct integration of eq 4 with a fourth-order Runge−Kutta routine, are presented in Figure 4.

Figure 4A shows the calculated acoustic grating signal for MbCO and deoxy Mb with parameters appropriate for the 585 nm probe grating experiment ($\tau_{ac} = 125$ ps from the acoustic maxima, and $\tau_{pulse} = 600$ fs). The acoustic grating signals were normalized for comparison. The dotted line is the deoxyMb thermal wave calculated with $1/\gamma = 8$ ps (eq 3). This signal amplitude is zero at $t = 0$ and reaches a maximum at 70 ps; the corresponding signal with $1/\gamma \sim 0$ ps reaches a maximum at 62.5 ps. The solid, dash, and dot−dash lines are the calculated MbCO acoustic responses with structural relaxation times of 0, 2, and 4 ps, respectively (eq 4). The acoustic signal driven by the instantaneous structural relaxation reaches a maximum at 62.5 ps, while the acoustic signal driven by the 2 ps structural relaxation reaches a maximum at 64.5 ps, and the 4 ps relaxation leads to a maximum at 66.5 ps. These results illustrate that a structural relaxation time of ~2 ps is required in order to observe the 6 ps phase shift of the protein wave relative to the deoxyMb acoustics. In Figure 4B, the calculated acoustic response of the protein wave with $\tau_{SR} = 2$ ps is compared with the MbCO grating signal (circles), and the calculated thermally generated acoustics are compared to the deoxyMb grating signal (triangles). The error bar of the fit can be inferred from Figure 4A.

The most important finding is that the protein strain evolves with a time constant on the order of 2 ps. This determination is independent of the above analysis. The phase shift, relative to a known response function, gives a direct experimental determination of this point. Equally important, by monitoring the phase shifts at approximately one-half acoustic cycle from $t = 0$, this study avoids the complications of spectral shifts that occur predominantly within the first few picoseconds[23] and

unambiguously demonstrates the initial protein motion involves strain developing on a 1−2 ps time scale. This observation is important as it gives a direct observation of the protein acoustic modes coupled to the reaction coordinate. In order for the protein relaxation to excite acoustics at the grating wavevector, the protein motion must lead to a volume change (strain) which involves translational motions. Furthermore, the additional constraint that this translational motion occur within 2 ps demonstrates that this motion involves a collective mode of the protein. This conclusion is based on speed of sound estimates for the protein. The speed of sound in the protein is not well-defined but should fall within $(1-2) \times 10^5$ cm/s. This range corresponds to typical speeds of sounds for liquids and glasses. Using a radius of 15 Å and this range of acceptable sound velocities gives an estimate of 1−2 ps for translational motion driven by a central force. Alternatively, one can describe this acoustic displacement within a modal description which, as discussed above, is more appropriate on this time scale. The time scale of 2 ps corresponds approximately to the effective half-period of the lowest frequency collective modes of myoglobin[8,46] which correspond to acoustic-like modes of the protein. Thus, the translational displacements on this time scale are too fast to be diffusive processes. This relaxation process is best described within a collective mode basis to properly convey the highly correlated nature of the motion.

The above study has demonstrated that the protein relaxation involves the displacement of translational or acoustic-like modes of the protein on a picosecond time scale. The resolution of this experiment is limited in time resolution by the signal-to-noise. There are undoubtedly higher frequency components involved in the bond-making/breaking process which are not observed in this experiment. In an effort to cast out the higher frequency modes, we examined the anisotropy of the evolving protein strain. The basic concept behind this experiment is similar to nonresonant studies of the Raman-active intermolecular modes of liquids. In experiments such as optical Kerr effect (OKE) spectroscopies, a short, nonresonant, polarized, laser pulse is used to displace the liquid modes through the forces generated by the differential polarizability or Raman effect.[18,47,48] The anisotropy in the induced nuclear polarization is probed by polarization-sensitive probes. In the present experiment, resonant-polarized excitation pulses are used to dissociate the ligand and preferentially select heme proteins with the heme plane parallel to the excitation polarization. The ensuing protein response is followed by probing the induced changes in birefringence in an analogous fashion to the OKE experiment. However, in this case, the force is generated by the reaction forces involved in the bond-breaking event, rather than the laser field. Since the protein environment is asymmetric by design, the reaction forces will lead to anisotropic displacements of the protein modes which will induce birefringence in the sample. In this manner, we should be able to cast out all the anisotropic modes and relaxation processes coupled to the ligation coordinate, at least up to times as long as the rotational depolarization times of the protein. The only question is how large is this effect relative to the birefringence that accompanies the changes in absorptive properties of the sample. On the basis of the large protein acoustic contributions observed even for resonant probes (see Figure 2), it might be expected that structural induced birefringence would dominate for off-resonant probes.

This expectation was in fact borne out. Results are shown in Figure 5 for grating excitation at 380 nm with different probe polarizations relative to the excitation at a probe wavelength of 760 nm. Scans out to 2 ns are shown so that two complete

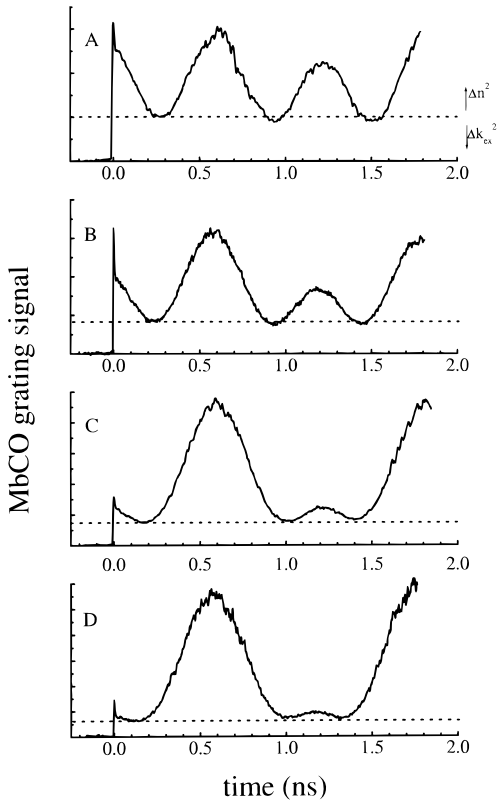

Figure 5. Polarization analysis of the protein phase grating contribution. The excitation wavelength was 380 nm, and $\theta_{ex} = 11°$. The probe wavelength was 760 nm. (A) Probe polarized parallel to the excitation. (B) Probe polarized at an angle of 30° to the excitation. (C) Probe polarized at an angle of 60° to the excitation. (D) Probe polarized perpendicular to the excitation. The dashed lines show the level of the amplitude contribution to the grating signals as indicated in (A).

acoustic modulations of the signal can be observed. At this excitation wavelength and an angle of 11°, the fringe spacing is 1.98 μm which, based on the speed of sound for water in this frequency range (1.55×10^5 cm/s), gives an acoustic period of approximately 1.28 ns. At the probe wavelength of 760 nm, there is a small-amplitude grating contribution due to the weak absorption of band III of the photogenerated deoxyMb. The acoustics only contribute to the phase component to the grating diffraction (eq 1). The amplitude component to the grating signal can be directly determined from the signal shown in Figure 5 as the point at which the acoustics completely cancel all phase grating components and produce double modulations in the signal per acoustic cycle.[13] The amplitude contribution is delineated in Figure 5 by the dashed line which makes this point clear. Thus, the amplitude grating contribution can be readily separated from the phase grating contributions at these experimental parameters. In addition, the maximum to the thermal contribution to the signal can be readily identified by the acoustic phase. The thermal response has an initial maximum at one-half an acoustic cycle from $t = 0$ and first manifests its effect at $t = 0.64$ ns and exhibits maxima every 1.28 ns from this time point. The exact positions of the thermally generated acoustics are readily observed by comparing the deoxyMb data to the MbCO data, as shown in Figure 2.

The thermally excited acoustics arise from the rapid nonradiative relaxation of the heme protein through collision-exchange processes with the surrounding water.[34] The expansion is determined almost exclusively by the water; the protein contributes less than 1% to the thermal expansion (by mass). Since the thermal expansion coefficients of liquids are isotropic

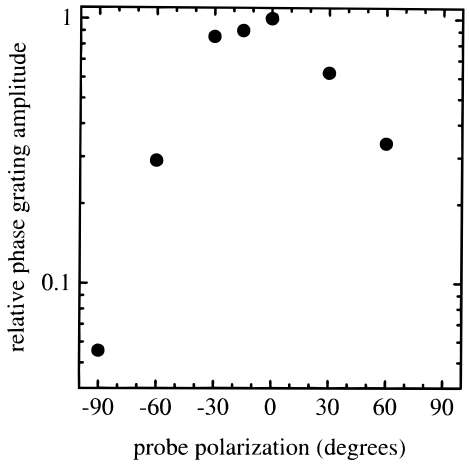

Figure 6. Phase grating signal as a function of probe polarization. The amplitude grating component has been subtracted from the diffracted signal.

by definition, the amplitude of the thermal contribution is polarization independent and can be used for internal calibration for birefringence effects arising from structural changes. This point was verified by conducting a probe polarization analysis of the thermally driven acoustics using deoxyMb under identical conditions. The acoustics were completely independent of probe polarization and were identical in waveform to that shown in Figure 2 for deoxyMb. From this consideration, it is immediately apparent from the data shown in Figure 5 for MbCO that there is a significant polarization dependence in the protein strain. For probe polarization parallel to the excitation, the acoustic amplitudes of the protein and thermal waves appear to be approximately equal. In contrast, as the probe polarization is rotated relative to the excitation, the apparent amplitude of the protein wave decreases and almost vanishes for the probe polarization perpendicular to the excitation. In addition, the amplitude of the acoustic modulation associated with the protein strain increases with time for the perpendicular polarization and shows a corresponding decrease in amplitude for the parallel polarization. This feature can be discerned from the maxima in the protein acoustics at positions $t \sim 0$ and $t = 1.28$ ns. The dynamics in the perpendicular and parallel probe polarizations are approximately the same as the rotation time of myoglobin in aqueous solutions. There may be nanosecond anisotropic relaxation components to the protein response which also contribute, but the dynamic range is too limited to clearly distinguish these components from rotational diffusion of the protein.

The most interesting observation is the magnitude of the anisotropy in the phase component. The excitation at 380 nm involves the Soret and N band of the heme porphyrin which are both in-plane *x*,*y*-polarized transitions.[49] The 760 nm probe transition is also an in-plane transition which is *x*,*y*-polarized.[49] The heme transitions are examples of a circular absorber which has a maximum anisotropy of 0.1 in absorption.[50] Using the Kramers−Kronig relationship for the associated phase, it can be shown that there is a corresponding effect in the dispersive contributions originating from the heme transitions. The magnitude of the index of refraction contribution to the diffracted signal, measured near the first maximum of the protein contribution ($t = 30$ ps), is shown as a function of probe polarization in Figure 6. Taking into account the quadratic scaling of the grating, the difference in the index of refraction changes (due to contributions from the protein strain) is ≥ 4 times larger in the parallel direction than in the perpendicular direction. The magnitude of this effect is far too large to be

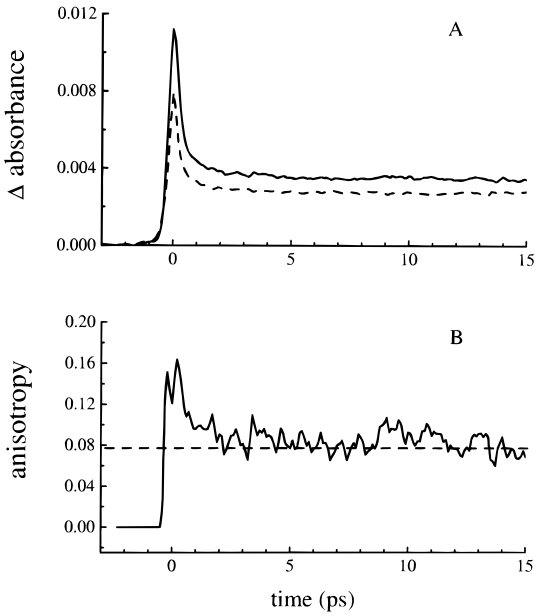

Figure 7. Absorption anisotropy measurement of MbCO. (A) Direct comparison of the changes in probe transmission at 760 nm for parallel (—) and perpendicular (- - -) polarizations, relative to the excitation polarization at 380 nm, in a pump/probe configuration. (B) Calculated absorption anisotropy from the above measurement.

attributable to induced absorption changes and accompanying changes in the index of refraction at the probe wavelength. Even a linear transition could only give rise to a induced effect on the absorption anisotropy of 0.4, which would correspond to a factor of 3 difference in index of refraction differences between the two polarization components. This statement is based on the assumption of a random distribution in which the only effect of absorption is to reduce the number density of absorbers at a particular transition. The protein relaxation involves a three-dimensional volume element such that the relaxation and development of strain will affect the sign and amplitude of the strain along all three axes. For example, stress applied along one axis of a finite volume element of even an isotropic material (free boundary condition) leads to compression along the direction of the applied stress and opposing dilation along the two orthogonal axes. The corresponding change in index of refraction would be opposite in sign along the direction of the stress and the two orthogonal components. The anisotropic motion of the protein in response to the reaction forces is analogous to this case, and the resultant birefringence would be larger than that possible from bleaching an optical transition. The results in Figures 5 and 6 clearly demonstrate this point.

To further ensure that the degree of birefringence is not due to transient changes in absorption, the absorption anisotropy for the same excitation and probe wavelength conditions was determined. The absorption anisotropy is defined as $(\Delta A_{||} - \Delta A_{\perp})/(\Delta A_{||} + 2\Delta A_{\perp})$ where $\Delta A_{||}$ and $\Delta A_{\perp}$ are the photoinduced absorption changes measured with parallel and perpendicular polarized probes, respectively. These results are shown in Figure 7. From the K−K analysis, the dominant contribution to the phase grating signal from photoconversion of MbCO to deoxyMb should come from the Soret band at 420 nm. Previous studies have shown that the photoinduced absorption anisotropy at this wavelength is approximately 0.1 for MbCO as expected for an *x*,*y*-polarized transition.[51] On a quantitative level, the anisotropy was found to be 0.09 ± 0.003 within the 10 ns resolution of this previous work. The slightly smaller than expected anisotropy was believed to arise from a slight rotation

of the heme plane within the heme pocket which accompanies protein relaxation.[51] The probe wavelength of the grating studies is resonant with the band III transition, which is a charge-transfer transition. The asymmetric structure of the heme pocket would act to break the symmetry of both the excitation and probe transitions and could lead to a larger anisotropy than expected for a strictly circularly polarized transition. Such an effect could be larger for band III and may be partially contributing to the observations shown in Figure 5.

The transient absorption anisotropy measurements (Figure 7) find that the anisotropy is very similar to that found earlier for probe wavelengths in the Soret region. There is an initial anisotropy which is larger than 0.1 and approaches 0.15. This anisotropy decays to a value of 0.08 ± 0.005 within 1 ps and remains essentially constant thereafter. The fast initial decay may have contributions from the electronic hyperpolarizability that would lead to the larger than expected anisotropy near $t = 0$. This contribution only occurs within the pulse width such that the anisotropy is still larger than expected and is approximately 0.12 after the first few hundred femtoseconds. There may be excited state contributions as well. However, the initially induced anisotropy due to these electronic transitions is related to the ground-state transition at 380 nm. Even for a polarized excited-state transition, the optical preparation from the ground state can only produce a maximum anisotropy of 0.1 for a perfectly circular *x*,*y*-polarized transition. On this basis, we believe that the initial anisotropy is larger than the expected 0.1 ($t > 300$ fs) value due to symmetry-breaking effects of the local protein structure, and the picosecond decay component is due the relaxation of the protein which leads to a slight rotation of the heme and commensurate reductions in the absorption anisotropy. This argument is further strengthened by recent transient Raman studies of the proximal histidine, a key marker of protein relaxation at the heme site, which find similar dynamics.[52] The contributions from the electronic hyperpolarizability and short-lived excited states make it difficult to quantify the exact, initial, anisotropy such that it is not possible to determine the average rotation angle that would be required to produce this decay. It is also noteworthy that the anisotropy relaxes to a value of 0.08 ± 0.005 as this value is very close to the value found previously with 10 ns pulses, probing the Soret and Q-band region, under the same excitation conditions. This work concluded that the protein relaxation coupled to the rotation of the heme ring is complete on a subnanosecond time scale. The present findings suggest that this motion is complete within 1−2 ps. This point needs to be revisited with larger dynamic range and better signal-to-noise to be conclusive. In relation to the grating studies, the most important observation is that the absorption anisotropy, even for band III, is on the order of 0.1 or less in the dynamic window of interest. Absorption anisotropy effects cannot account for the large induced birefringence observed. The birefringence must be due to anisotropic material displacements involved in the protein relaxation.

The realization that the protein strain leads to significant birefringence offers new insight into the acoustic detection of the protein motion. For most grating, generated acoustics, the first maximum in the diffracted signal occurs at one-half an acoustic cycle from $t = 0$. The thermally driven sound waves for photoexcited deoxyMb illustrate this behavior. This effect is a consequence of the inertial effects on the sound wave excitation. The vibrational relaxation to translational (and rotational) degrees of freedom of the bath is imaged into a velocity gradient of the grating period which gives a $t = 0$ stress boundary condition.[44] The ensuing material expansion occurs at the speed of sound but requires a half-period to reach its full value with respect to the grating period for light diffraction. In contrast, the protein strain reaches its maximum effect on the diffracted probe on picosecond time scales. The rapid index of refraction changes that accompany the protein structural changes was shown by a detailed probe wavelength dependence to arise from the protein contribution to the index of refraction, i.e., could not be explained by population contributions.[13] This result indicated that the diffraction process was determined by material displacement associated with the protein dynamics and not by the grating period. Puchenkov and Malkin have examined this problem theoretically and shown that with a time-dependent volume change (eq 4) there is an acoustic field excited at the grating wave vector in agreement with the experimental findings.[45] This theory did not, however, include the effects of the protein structural changes on the nonpropagating component to the index of refraction modulation. This term needs to be included. For example, in the thermal grating case, the sample's temperature is modulated, which in turn leads to a modulation in the index of refraction through thermal expansion. This term is nonpropagating and only decays with thermal diffusion. The thermally driven acoustics (propagating term) beat against this offset which leads to the observation of one acoustic modulation of the signal per acoustic cycle. In the same manner, the change in protein structure leads to material strain and a nonpropagating term to the index of refraction modulation. The observation of birefringence with the acoustic generation confirms this point. It is clear from the induced birefringence that the protein relaxation is leading to a larger, net, mass displacement parallel to the excitation's polarization than in the perpendicular direction. This motion leads to a differential change in the index of refraction of the correct periodicity for light diffraction and accounts for the rapid rise time in the grating diffraction. The acoustics are driven by the protein motion which also involves a volume change. The acoustics beat against the nonpropagating periodic modulation in the index of refraction, derived from the protein's anisotropic strain. To be specific, the approximate $t = 0$ strain boundary condition for the protein is imaged by the light intensity pattern into a sinusoidal stress condition at the grating wave vector. This sinusoidal force generates the acoustics which then beat against the nonpropagating, anisotropic, protein contribution to the index of refraction. The anisotropy or birefringence in this term decays with the rotation of the protein.

The direct observation of the anisotropic displacement in response to the reaction forces offers a new probe of mode-specific couplings. Despite the inherent time resolution of this technique, the underlying amplitude grating contribution and short-lived excited-state contributions make it difficult to extract the early time dynamics of the protein relaxation to make this connection. To further enhance the resolution of the dynamics behind this motion, direct comparisons between MbCO and carboxyheme octapeptide (HOPCO) were conducted. Heme octapeptide is the intact heme pophyrin ring with a polypeptide chain bonded to the ring. The volume changes associated with the photodissociation of the CO for HOPCO are much smaller than mediated in the presence of the protein, and only the thermally generated acoustics are observed. The HOPCO and MbCO grating signals, taken under identical conditions, are shown in Figure 8. The signal is very similar to MbCO, except the phase contribution due to the protein-induced strain is significantly larger for the probe polarized parallel to the excitation for MbCO than that observed for HOPCO. These

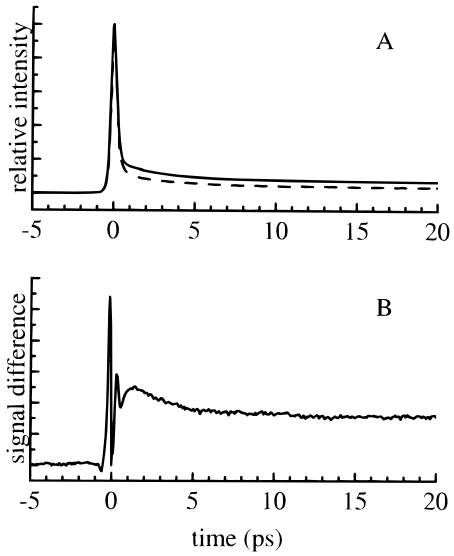

Figure 8. Short time dynamics of the protein anisotropic strain. (A) MbCO (—) is compared to hemeoctapeptide (- - -) using 380 nm excitation ($\theta_{ex} = 4.5°$) and a 760 nm probe under the same conditions. (B) Difference in the diffracted grating signal (from A) observed for MbCO and HOPCO.

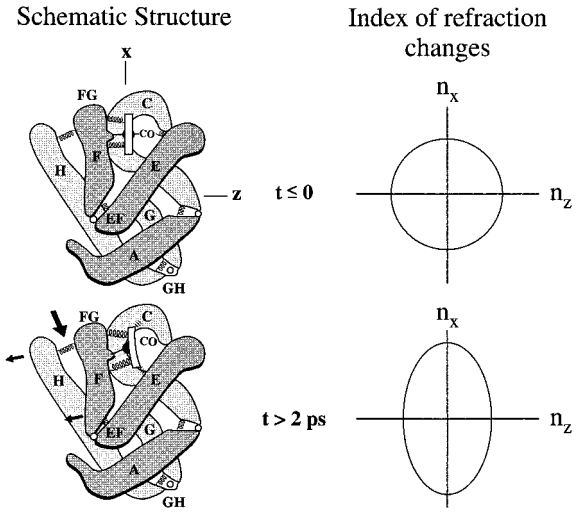

Figure 9. Schematic drawing of the short time dynamics of the functionally important protein motions. Top: MbCO prior to the optical initiation of the oxy to deoxy structure transition. The index of refraction of the medium (right panel) is isotropic at this point. Lower: photodissociation of CO leads to a force on the surrounding globin through the doming of the heme (dark semicircle = Fe). The reaction force displaces the various helical sections as a collective motion as shown; i.e., the helical sections are modeled as rigid bodies relative to the looped sections which serve as hinges for the displacements. The arrows indicate the direction of displacement inferred from equilibrium differences in the oxy and deoxy structures of myoglobin (refs 1, 8, and 63). The largest tertiary structural changes involve the F α-helix which moves parallel to the heme and a repositioning of 75% of the protein atoms, on the proximal side of the heme. There are smaller motions throughout the protein (not shown). The anisotropic force/displacement was observed through polarization analysis of the phase grating component. The index of refraction change was largest along the direction parallel to the heme plane (right panel), which indicates larger mass displacements along this coordinate. This motion can be viewed as the displacements of a superposition of the lowest frequency collective modes of the protein.

data show the total grating signal. The difference would be even greater if the phase component alone was compared.

Using the HOPCO results as a baseline for the heme photophysical processes, the protein dynamics can be highlighted by plotting the difference between the two sets of data. This comparison is shown in Figure 8B. The rapid modulation near $t = 0$ is due to the subtraction of a rapidly changing signal component. This is followed by a 4−5 ps decay component which is due to vibrational cooling contributions to both the phase and amplitude components of the grating which are not removed in plotting the difference in signal amplitudes between HOPCO and MbCO. This decay component is identical to control studies of the deoxy analogues and is in agreement with other determinations of the vibrational cooling.[26,53] The vibrational cooling dynamics, unfortunately, mask the protein relaxation processes that might otherwise be observable in this time window by such a comparison. However, there is an approximately 1 ps rise in the signal of MbCO relative to HOPCO. The rise time is related to the larger phase contribution observed for MbCO relative to HOPCO and represents the protein relaxation that is absent in the HOPCO control. This feature to the data is observable between $t = 0.5$ and 1.5 ps and is consistent with the results determined from the counterpropagating grating studies. The most important conclusion to be drawn from these data is that the anisotropic strain that develops with protein relaxation occurs on a picosecond time scale and appears to be the largest component to the protein strain.

To provide a unifying picture for the different measurements within a microscopic model for the protein relaxation, the protein structural changes and connection to the observables are shown schematically in Figure 9. This figure shows the anisotropic displacement of the different helices in response to the reaction forces. The relative displacements are based on the differences in equilibrium structures between MbCO and deoxyMb. The anisotropic nature of these displacements was clearly observed in the induced birefringence. This motion involves the coupling of the reaction forces to acoustic-like modes of the protein and the development of strain local to the protein. The protein strain develops on a picosecond time scale and creates a sinusoidal stress boundary condition at the grating wave vector that generates the acoustics. The coupling of the bond breaking to the collective, nondiffusive, modes of the protein was directly observed in the counterpropagating grating studies of the protein-generated sound waves (Figure 3). This study illustrated that the initial protein relaxation involves the displacement of acoustic-like modes of the protein. The anisotropy of the mass displacement (Figure 5) and supportive dynamical studies (Figure 8) were provided by polarization analysis of the induced birefringence in the phase grating components (observed for MbCO, absent for deoxyMb and HOPCO). The absorption anisotropy studies of the heme transition at 760 nm (Figure 7) further confirmed that the observed birefringence was not due to electronic effects but to the protein motion.

IV. Concluding Remarks

The general phenomenon of molecular cooperativity in biological systems involves the coupling of two or more reaction coordinates. The allosteric regulation of the oxygen binding at the heme sites in hemoglobin is a classic example of this general phenomenon. In order for the binding of oxygen at one heme site to affect its neighbors, the reaction forces at the heme binding site must lead to atomic displacements at the protein interface, i.e., the development of strain along the coupled reaction coordinate. Given the enormous number of degrees of freedom available to the molecule, the atomic displacements

involved in molecular cooperativity cannot arise from a random search of all the available phase space. The reaction forces must be highly directed by the anisotropic three-dimensional structure of the protein. The mechanism by which the reaction forces, which initially develop on an atomic length scale, ultimately drive displacements on the mesoscopic length scale appropriate to biological functions is a key issue in understanding biological functions from a fundamental standpoint.

Ideally, one would like to follow the entire series of events leading up to the structural changes that constitute the molecular communication pathway, from the bond-breaking event to the full structural relaxation along the reaction coordinate. Two different experimental approaches were developed to directly follow the time evolution of the protein strain using MbCO as a model system for the tertiary motions involved in the allosteric control of oxygen binding in hemoglobin. The time resolution of these methods with respect to this observable is unprecedented and was sufficient to follow the coupling of the reaction coordinate to the inherent low-frequency modes of the protein, i.e., the initial barrier crossing dynamics.

From the phase of the protein driven acoustics, the counter-propagating grating studies have determined that the bond dissociation involves a translational displacement of an acoustic-like mode of the protein within 2 ps. This conclusion is based on (1) the fact that the protein motion couples to the hydrodynamic acoustic modes of the grating wavevector and (2) the time scale for this protein volume change. The former point illustrates that this motion is not localized but involves a global volume change of the protein. This in turn illustrates that the motion involves translations. The collective nature of this motion is demonstrated by the observed dynamics. The dominant component to the protein strain is developing essentially at the speed of sound and is too fast to be a diffusive process. This motion is best described within a modal basis in which the reaction forces derived from the Fe−CO bond dissociation are coupled to the low-frequency collective modes of the surrounding globin. Assuming linear response, the atomic displacements would occur on a time scale comparable to a half-period of the modes with the largest displacements. From a normal-mode treatment of the tertiary structure differences between MbCO and deoxyMb, a theoretical analysis has shown that more than 60% of the structural differences can be reconstituted by the displacement of four modes in the range $5-12\ cm^{-1}$.[8,46] The effective half-period of these modes is very close to the experimental observations. This theoretical study should give a reasonable approximation of the lowest frequency modes. Again, the main point is that there is a global volume change which is occurring at the speed of sound. This observation defines a collective response.

In terms of the functionality of the protein, the 3-dimensional structure of the protein is highly anisotropic and should be integral to directing the reaction forces to specific motions important to the protein function. This expectation was borne out. Polarization analysis of the phase grating components due to the protein strain found the strain to be highly anisotropic, as evidenced by the significant induced birefringence in the sample. There has been a considerable effort made in trying to obtain microscopic details on the specific modes coupled to reaction coordinates in condensed-phase systems.[15−21,54,55] Quantifying the coupling coefficients to specific modes provides a microscopic view of the reaction coordinate in an otherwise complex system.[55] The details of mode-specific couplings become more important in biological systems as the very function of the molecule relies on these details. The highly anisotropic force distribution inherent in the protein structure leads to a clearly observable birefringence. The dynamics of the induced birefringence can be directly related to the modes coupled to the reaction coordinate and in principle the coupling coefficients. In the present study, short-lived excited-state transitions of the heme group and complications from vibrational cooling made it difficult to extract the short time dynamics. However, it was possible to determine that the anisotropic strain components in the protein structure have an approximately 1 ps component which becomes fully developed within 5 ps. These dynamics are consistent with the grating photoacoustics. Moreover, the largest net mass displacement (increase in the index of refraction) is in the direction parallel to the heme plane. This motion and ensuing birefringence are most likely related to the translational motion of the EF helical section. From X-ray crystal stucture determinations and difference mapping, one of the largest displacements involved in the tertiary structure changes occurs at the proximal histidine ligation site to the heme.[1,2] The breaking of the Fe−CO bond leads to the doming of the iron out of plane and a tilting of the proximal histidine with a corresponding translation of the EF helix, in a direction with the largest component parallel to the heme plane. It is difficult to determine from the X-ray data whether this motion involves a net contraction, as observed experimentally in solution, but the highly anisotropic nature of the displacement is consistent. This particular detail in the protein relaxation is often referred to as the allosteric core.[4] The reaction forces are viewed to be directed to the protein interface along this coordinate.[2−4] The phase grating studies have directly observed anisotropic strain consistent with this concept.

The other, more rigorous, test for collective mode coupling is the correlation of motion over two different length scales. The phase grating measurements are sensitive to the long length scale of the protein motion, whereas the relaxation at the heme site is most sensitive to short-range motion closest to the epicenter of the reaction forces. Previously, we have made this connection but could only state that the global protein motion occurs within an order of magnitude of relaxation processes near the heme binding site.[7,13] The most recent work of Franzen et al. has shown that the proximal histine relaxation, which is the closest contact point of the protein to the heme, occurs on a 1 ps time scale.[52] Similarly, studies of band III, which is sensitive to the out-of-plane motion of the iron, have observed that the dominant relaxation component, which is sensitive to the surrounding solvent viscosity (i.e., involves a volume change), has a 2−4 ps dynamical signature.[26] Our current results of the absorption anisotropy of band III find a smaller anisotropy than expected for heme transitions. From the earlier analysis of Ansari and co-workers,[51] this result suggests that the relaxation involving rotation of the heme plane, which accompanies the translation of the EF helix, occurs on this 1−2 ps time scale. Based on these series of independent probes of the relaxation at the heme site and the grating studies of the global protein motion, there is essentially a 1:1 correspondence in motion over two different length scales of motion. The two-point spatial correlation of the dynamics illustrates the collective aspects of the motion and demonstrates the involvement of collective modes in the initial propagation of the structure changes.

The other important detail in these findings is that the largest displacement along the protein strain coordinate occurs through the displacement of the collective modes. Our previous studies found that greater than 80% of the protein strain developed during this initial phase of the protein relaxation.[12,13,42] The

earlier studies were restricted to a dynamic window from 10 ps to 10 ns. The present results demonstrate that the initial relaxation phase does occur through coupling of the reaction forces to the inherent collective modes of the protein, and the dominant strain develops within 2 ps. We have also extended the time base out to milliseconds,[56] and it is clear that this initial relaxation process accounts for most of the protein relaxation out to several hundred nanoseconds, after which ligand diffusion begins to contribute. Assuming linear response, the relaxation energetics should scale quadratically with displacement. With this connection between strain and energetics, these results indicate that the initial nondiffusive motions of the protein account for greater than 50% of the relaxation energy associated with the bond-breaking event. This conclusion is supported by direct studies of the relaxation energetics, through the thermal component to the phase grating signal, which have found that the protein has essentially relaxed within 100 ps.[7,13] The thermal measurements, however, did not have sufficient time resolution or dynamic range to fully determine the relative degree of relaxation. With the current time resolution and dynamic range, it is clear that the largest coupling coefficients of the bond dissociation coordinate are to the collective, nondiffusive, modes of the protein. This collective mode mechanism is shown schematically in Figure 9.

These findings should be compared to other studies of the heme protein dynamics. Most of the studies have focused on optical probes of the heme site. After photodissociation, there is an evolution of the heme absorption spectra to that of the fully relaxed deoxymyglobin occurring over several decades in time.[6,14,25−30,57] The details of the relaxation depend strongly on the viscosity of the solution, which is consistent with the phase grating studies which have illustrated that the relaxation involves volume changes or strain in the protein. The relative amplitudes of the various relaxation components depend strongly on the mechanical boundary conditions imposed by the surrounding fluid; i.e., the protein motion is "slaved" to the solvent.[58] In low-temperature glasses, the protein structural relaxation is completely blocked by the surrounding rigid matrix. The spectra of photogenerated deoxymyglobin relative to equilibrium deoxymyoglobin at liquid helium temperatures can be used as a reference for the electronic spectra of the heme in the absence of protein relaxation.[59] On this basis, studies of transient spectra in the Soret, Q-band,[14,25−28] and band III[26,60] of the heme transitions, in aqueous solution at room temperature, all show the largest relative spectral shift toward the fully relaxed deoxy spectrum in the first few picoseconds. Similarly, transient Raman probes of the proximal histidine show that the dominant relaxation component occurs on this same time frame.[52] Closely related experiments have been conducted using impulsive Raman scattering which have found evidence for coherent propagation along the reaction coordinate with respect to the heme porphyrin vibrational modes.[61] The recent time-resolved X-ray diffraction studies have similarly found significant structural changes within the current 10 ns resolution limit.[62] Clearly large-scale structural changes have occurred in order to be observable within the 1.8 Å resolution of the X-ray diffraction experiments.

From these various studies, it is apparent that the protein relaxation extends over several decades in time. Most of the attention has focused on the highly distributed dynamics involved in geminate recombination of the CO and other ligands and the nonexponential relaxation phase at the heme site which is reminiscent of glass relaxation dynamics.[6,25−30,57,58] The focus on the long time limit of the protein relaxation has led to the view that the dominant relaxation mechanism involves conformational relaxation. However, even in these studies, the largest relaxation component occurred either faster than the experimental resolution or within the first few picoseconds (for aqueous systems). Thus, the present work is completely consistent with this body of work and explains the underlying mechanics responsible for the large initial relaxation. The largest coupling coefficient of the reaction coordinate is to the nondiffusive collective modes of the protein.

Both the dynamics and magnitude of the strain components are important findings. This work establishes that the largest coupling coefficient of the iron ligation coordinate is to the nondiffusive collective motions of the protein. In order for the protein to perform its function, the energetics of the reaction coordinate must be highly directed to the motions important to its function. The propagation of the tertiary structural changes through the displacement of collective modes represents the most efficient mechanism possible for executing these motions; i.e., the atoms involved are displaced as a unit without intermediate steps during this phase of the motion. This mechanism avoids the problem of entrapment in local minima. It is undoubtedly no coincidence that the collective mode mechanism of force displacement plays a significant role in structural relaxation. Secondary structures such as helices and β sheets abound in nature. These structures provide relatively rigid elements in the protein architecture[7,8,12] which enhance the coupling to collective motions by the high degree of correlated motion orchestrated through the primary and secondary structure. Evolutionary pressures which create looped sections or other disordered sections in the three-dimensional structure act as hinges for the correlated motion of the more rigid, ordered, secondary features and enable the system to highly direct the reaction forces. In this manner, the protein structure is able to reduce the number of labile coordinates in the reaction coordinate, reducing significantly the thermal sampling of spurious conformations that do not contribute to function. After this nondiffusive motion along the reaction coordinate, the specific details of the conformational substates will determine the final phase of the structural changes important to function, whereas the collective mode mechanism directs the overall process along the correct seam in a highly complex potential energy surface. Simply put, these observations further illustrate how fully optimized reaction coordinates are in biological systems.

As a final comment, there are obvious extensions of this work to other chemical reactions. There is, however, a distinct advantage with biological systems in that the inherent heterogeneous structure of these systems enables a separation of length scales (**k** dependence) of relaxation convolved to the reaction coordinate. For this reason, our most detailed understanding of condensed-phase reaction dynamics may come from studies of biological systems. It would be interesting to extend this approach to other biological systems such as rhodopsin, bacteriorhodopsin, and photosynthetic reaction centers where the protein is thought to play a critical role in determining the reaction pathway. Key questions revolve about the importance of the protein dynamics versus static asymmetries at the reaction site in directing the process. Higher sensitivity to specific modes is needed to resolve some of the issues. The next major step forward will be the development of methodologies that enable the separation of the short time dynamics of excited-state processes from the protein contribution to the signal. Optical heterodyne detection and separation of the real (phase) and imaginary (amplitude) components to the grating would both

improve the sensitivity by several orders of magnitude and provide a scaling parameter (Δn_{ex} can be correlated to Δk_{ex}) for subtracting excited-state contributions to the phase. Without the complications from excited-state contributions, it should be possible to attain very high sensitivity to mode specific couplings of the reaction coordinate. In addition, the significant improvements in time resolution to the photoacoustics now enable direct determination of the reaction energetics with picosecond time resolution. This new capability will make it possible to determine reaction energetics and answer important questions with respect to the driving force and relative positions of intermediate states in the cascaded steps generally found in biological systems. It will also be very informative to extend the time base out to milliseconds and longer to make a continuous connection between the short time and long time behavior. Work along these lines will provide an extremely sensitive probe of the complete range of motions relevant to biological functions.

Acknowledgment. This work was supported by the National Institute of Health and the Natural Sciences and Engineering Research Council of Canada. We thank Vladimir Astinov and Greg Goodno for helpful discussions and assistance with the latter stages of the femtosecond studies.

References and Notes

(1) Dickerson, R. E.; Geiss, I. *Hemoglobin: Structure, Function, Evolution, and Pathology*; Benjamin Cummings: Menlo Park, CA, 1983.
(2) Perutz, M. F. *Nature* **1970**, *228*, 726.
(3) Freidman, J. M.; Scott, T. W.; Fisanick, G. J.; Simon, S. R.; Findsen, E. W.; Ondrias, M. R.; MacDonald, V. W. *Science* **1985**, *229*, 187.
(4) Gelin, B. R.; Karplus, M. *Proc. Natl. Acad. Sci. U.S.A.* **1977**, *74*, 801.
(5) Monod, J.; Wyman, J.; Changeux, J. P. *J. Mol. Biol.* **1965**, *12*, 88.
(6) Frauenfelder, H.; Sligar, S. G.; Wolynes, P. G. *Science* **1991**, *254*, 1598.
(7) Miller, R. J. D. *Acc. Chem. Res.* **1994**, *27*, 145.
(8) Seno, Y.; Go, N. *J. Mol. Biol.* **1990**, *216*, 95.
(9) Cusack, S.; Doster, W. *Biophys. J.* **1990**, *58*, 243. Kurita, A.; Shibata, Y.; Kushida, T. *Phys. Rev. Lett.* **1995**, *74*, 4349.
(10) Miller, R. J. D.; McLendon, G.; Nozik, A. J.; Schmickler, W.; Willig, F. *Surface Electron Transfer Processes*; VCH: New York, 1995; Chapter 3, p 74.
(11) Auld, B. *Acoustic Fields and Waves in Solids*; Wiley: New York, 1973.
(12) Genberg, L.; Richard, L.; McLendon, G.; Miller, R. J. D. *Science* **1991**, *251*, 1051.
(13) Richard, L.; Genberg, L.; Deak, J.; Chiu, H. L.; Miller, R. J. D. *Biochemistry* **1992**, *31*, 10703.
(14) Haugen, S. J.; Eaton, W. A. *J. Chem. Phys.* **1996**, *90*, 3395 and references therein.
(15) Keyes, T. *J. Chem. Phys.* **1994**, *101*, 5081.
(16) Stratt, R. M. *Acc. Chem. Res.* **1995**, *28*, 201. Cho, M.; Fleming, G. R.; Saito, S.; Ohmine, I.; Stratt, R. M. *J. Chem. Phys.* **1994**, *100*, 6672.
(17) Ohmine, I.; Tanaka, H. *Chem. Rev.* **1993**, *93*, 2545.
(18) Palese, S.; Schilling, L.; Miller, R. J. D.; Staver, P. R.; Lotshaw, W. T. *J. Phys. Chem.* **1994**, *98*, 6308.
(19) Walfren, G. E. *J. Phys. Chem.* **1990**, *94*, 2237.
(20) Rosenthal, S. J.; Jimenez, R.; Fleming, G. R.; Kumar, P. V.; Maroncelli, M. *J. Mol. Liq.* **1994**, *60*, 25.
(21) Jimenez, R.; Fleming, G. R.; Kumar, P. V.; Maroncelli, M. *Nature* **1994**, *369*, 471.
(22) Gibson, Q. H.; Ainsworth, S. *Nature* **1957**, *180*, 1416.
(23) Petrich, J. W.; Martin, J. L. *Chem. Phys.* **1989**, *131*, 31.
(24) Straub, J. E.; Karplus, M. *Chem. Phys.* **1991**, *158*, 221.
(25) Ansari, A.; Jones, C. M.; Henry, E. R.; Hofrichter, J.; Eaton, W. A. *Biophys. J.* **1993**, *64*, 852.
(26) Jackson, T. A.; Lim, M.; Anfinrud, P. A. *Chem. Phys.* **1994**, *180*, 131.
(27) Agmon, N.; Doster, W.; Post, F. *Biophys. J.* **1994**, *66*, 1612.
(28) Lambright, D. G.; Balasubramanian, S.; Boxer, S. G. *Chem. Phys.* **1991**, *158*, 249.
(29) Shulman, R. G.; Hopfield, J. J.; Ogawa, S. *Q. Rev. Biophys.* **1975**, *8*, 325.
(30) Kaminaka, S.; Ogura, T.; Kitagawa, T. *J. Am. Chem. Soc.* **1990**, *112*, 23.
(31) Chernoff, D. A.; Hochstrasser, R. M.; Steele, A. W. *PNAS* **1980**, *77*, 5606.
(32) Jones, C. M.; Ansari, A.; Henry, E. R.; Christoph, G. W.; Hofrichter, J.; Eaton, W. A. *Biochemistry* **1992**, *31*, 6692.
(33) Miller, R. J. D. *Time Resolved Spectroscopy*; Clark, R. J. H., Hester, R. E., Eds.; Wiley: Chichester, England, 1989; Vol. 18, p 1.
(34) Miller, R. J. D. *Annu. Rev. Phys. Chem.* **1991**, *42*, 581.
(35) Zimmt, M. B. *Chem. Phys. Lett.* **1989**, *160*, 564.
(36) Hara, T.; Hirota, N.; Terazima, M. *J. Phys. Chem.* **1996**, *100*, 10194.
(37) Nelson, K. A.; Fayer, M. D. *J. Chem. Phys.* **1980**, *72*, 5202.
(38) Kraehenbuhl, J. P.; Galardy, R. E.; Jamieson, J. D. *J. Exp. Med.* **1974**, *139*, 208.
(39) Nelson, K. A.; Casalegno, R.; Miller, R. J. D.; Fayer, M. D. *J. Chem. Phys.* **1982**, *77*, 1144.
(40) Genberg, L.; Heisel, F.; McLendon, G.; Miller, R. J. D. *J. Phys. Chem.* **1987**, *91*, 5521.
(41) Westrick, J. A.; Peters, K. S.; Ropp, J. D.; Sligar, S. G. *Biochemistry* **1990**, *29*, 6741. Leung, W. P.; Cho, K. C.; Chau, S. K.; Choy, C. L. *Chem. Phys. Lett.* **1987**, *141*, 220.
(42) Deak, J.; Richard, L.; Pereira, M.; Chiu, H. L.; Miller, R. J. D. *Methods Enzymol.* **1994**, *232*, 322.
(43) Lian, T.; Locke, B.; Kholodenko, Y.; Hochstrasser, R. M. *J. Phys. Chem.* **1994**, *98*, 11648.
(44) Genberg, L.; Bao, Q.; Gracewski, S.; Miller, R. J. D. *Chem. Phys.* **1989**, *131*, 81.
(45) Puchenkov, O. V.; Malkin, S. *Chem. Phys. Lett.* **1996**, *251*, 242.
(46) Seno, Y.; Go, N. *J. Mol. Biol.* **1990**, *216*, 111.
(47) McMorrow, D.; Lotshaw, W. T.; Kenny-Wallace, G. A. *IEEE Quantum Electron.* **1988**, *24*, 443.
(48) Palese, S.; Mukamel, S.; Miller, R. J. D.; Lotshaw, W. T. *J. Phys. Chem.* **1996**, *100*, 10380.
(49) Eaton, W. A.; Hofrichter, J. *Methods Enzymol.* **1981**, *76*, 175.
(50) Magde, D. *J. Chem. Phys.* **1978**, *68*, 3717.
(51) Ansari, A. Jones, C. M.; Henry, E. R.; Hofrichter, J.; Eaton, W. A. *Biophys. J.* **1993**, *64*, 852−868.
(52) Franzen, S.; Bohn, B.; Poyart, C.; Martin, J. L. *Biochemistry* **1995**, *34*, 1224.
(53) Lingle, Jr., R.; Xu, X.; Zhu, H.; Yu, S.; Hopkins, J. B. *J. Phys. Chem.* **1991**, *95*, 9320.
(54) Lanzafame, J. M.; Palese, S.; Wang, D.; Miller, R. J. D.; Muenter, A. A. *J. Phys. Chem.* **1994**, *98*, 11020.
(55) Maroncelli, M.; Fleming, G. R. *J. Chem. Phys.* **1988**, *89*, 5044.
(56) Chui, H. L. Ph.D. Thesis, University of Rochester, 1995.
(57) Steinbach, P. J.; Ansari, A.; Berendzen, J.; Braunstein, D.; Chu, K.; Cowen, B. R.; Ehrenstein, D.; Frauenfelder, H.; Johnson, J. B.; Lamb, D. C.; Luck, S.; Mourant, J. R.; Nienhaus, G. U.; Ormos, P.; Philipp, R.; Xie, A.; Young, R. D. *Biochemistry* **1991**, *30*, 3988.
(58) Ansari, A.; Jone, C. M.; Henry, E. R.; Hofrichter, J.; Eaton, W. A. *Science* **1992**, *256*, 1796.
(59) Srajer, V.; Champion, P. M. *Biochemistry* **1991**, *30*, 7390.
(60) Xie, X.; Simon, J. D. *Biochemistry* **1991**, *30*, 3682.
(61) Zhu, L.; Li, P.; Haung, M.; Sage, J. T.; Champion, P. M. *Phys. Rev. Lett.* **1994**, *72*, 301.
(62) Srajer, V.; Teng, T.; Ursby, T.; Pradervand, C.; Ren, Z.; Adachi, S.; Schildkamp, W.; Bourgeois, D.; Wulff, M.; Moffat, K. *Science* **1996**, *274*, 1726.
(63) Kuriyan, J.; Wilz, S.; Karplus, M.; Petsko, G. A. *J. Mol. Biol.* **1986**, *192*, 133.